Topology of conical/surface intersections among five low-lying electronic states of CO2: Multireference configuration interaction calculations

Bo Zhou, Chaoyuan Zhu, Zhenyi Wen, Zhenyi Jiang, Jianguo Yu, Yuan-Pern Lee, and Sheng Hsien Lin

Citation: The Journal of Chemical Physics **139**, 154302 (2013); doi: 10.1063/1.4824483
View online: http://dx.doi.org/10.1063/1.4824483
View Table of Contents: http://scitation.aip.org/content/aip/journal/jcp/139/15?ver=pdfcov
Published by the AIP Publishing

Articles you may be interested in

A global ab initio potential energy surface for the X 2 A ground state of the Si + OH SiO + H reaction
J. Chem. Phys. **139**, 204305 (2013); 10.1063/1.4832324

Spin-orbit corrected full-dimensional potential energy surfaces for the two lowest-lying electronic states of FH2O and dynamics for the F + H2O HF + OH reaction
J. Chem. Phys. **138**, 074309 (2013); 10.1063/1.4791640

A theoretical approach to the photochemical activation of matrix isolated aluminum atoms and their reaction with methane
J. Chem. Phys. **133**, 174307 (2010); 10.1063/1.3499813

Transition probabilities for the Au (S 2 , D 2 , and P 2) with SiH 4 reaction
J. Chem. Phys. **132**, 044301 (2010); 10.1063/1.3298586

Analytic potential energy surfaces and their couplings for the electronically nonadiabatic chemical processes Na (3p)+ H 2 Na (3s)+ H 2 and Na (3p)+ H 2 NaH+H
J. Chem. Phys. **110**, 4315 (1999); 10.1063/1.478314

This article is copyrighted as indicated in the article. Reuse of AIP content is subject to the terms at: http://scitation.aip.org/termsconditions. Downloaded to IP: 140.113.38.11 On: Wed, 30 Apr 2014 06:05:21

Topology of conical/surface intersections among five low-lying electronic states of CO_2: Multireference configuration interaction calculations

Bo Zhou,[1,2] Chaoyuan Zhu,[1,a)] Zhenyi Wen,[2] Zhenyi Jiang,[2] Jianguo Yu,[3] Yuan-Pern Lee,[1] and Sheng Hsien Lin[1]

[1]*Department of Applied Chemistry, Institute of Molecular Science and Center for Interdisciplinary Molecular Science, National Chiao-Tung University, Hsinchu 30050, Taiwan*
[2]*Institute of Modern Physics, Northwest University, Xi'an 710069, People's Republic of China*
[3]*Department of Chemistry, Beijing Normal University, Beijing 100875, People's Republic of China*

(Received 16 April 2013; accepted 25 September 2013; published online 14 October 2013)

Multi-reference configuration interaction with single and double excitation method has been utilized to calculate the potential energy surfaces of the five low-lying electronic states $^1A_1$, $^1A_2$, $^3A_2$, $^1B_2$, and $^3B_2$ of carbon dioxide molecule. Topology of intersections among these five states has been fully analyzed and is associated with double-well potential energy structure for every electronic state. The analytical potential energy surfaces based on the reproducing kernel Hilbert space method have been utilized for illustrating topology of surface crossings. Double surface seam lines between $^1A_1$ and $^3B_2$ states have been found inside which the $^3B_2$ state is always lower in potential energy than the $^1A_1$ state, and thus it leads to an angle bias collision dynamics. Several conical/surface intersections among these five low-lying states have been found to enrich dissociation pathways, and predissociation can even prefer bent-geometry channels. Especially, the dissociation of $O(^3P) + CO$ can take place through the intersection between $^3B_2$ and $^1B_2$ states, and the intersection between $^3A_2$ and $^1B_2$ states. © *2013 AIP Publishing LLC*. [http://dx.doi.org/10.1063/1.4824483]

I. INTRODUCTION

The collisions of $O(^3P, ^1D)$ with $CO(^1\Sigma^+)$ have been widely studied both experimentally and theoretically.[1–6] A large amount of electronic energy can be efficiently transferred through a spin-orbit induced surface/conical intersection involving a long-lived (several vibrations) collision complex intermediates. The vibrational relaxation of $CO(^1\Sigma^+)$ by $O(^3P)$ is several orders of magnitude faster than predicted by the conventional theory of translational to vibrational energy transfer.[7] In CO_2 photodissociation experiments,[8] the dissociation at 185 nm is considered as a spin forbidden process which involves two steps: an electronic transition from the ground state ($1^1\Sigma^+$) to an upper bounded single state $^1B_2$ and then transition to an unbounded triplet $^3B_2$ state. The transition from the $^3B_2$ state back to the ground state can take place only in the presence of some perturbation such as spin-orbit couplings. However, the spin-orbital induced surface crossing between $^3B_2$ and $^1A_1$ states cannot explain an unusual enrichment of ^{17}O isotope.[9] Therefore, the topology of surface/conical intersections between the lowest electronic singlet and triplet states must play an important role for the dissociation mechanism of carbon dioxide molecule.

The conical/surface intersection problem of carbon dioxide molecule has attracted attention for high-level *ab initio* quantum chemistry calculations. Julienne *et al.*[10] have reported self-consistent-field and small configuration-interaction calculation of the potential energy curves along the bending coordinate for the four lowest bent singlet states. Simkin *et al.*[11] have calculated the potential energy surfaces (PESs) of the ground state ($^1\Sigma_g^+$) and excited electronic states ($^3B_2$, $^1B_2$), and their calculations indicated that no crossing point is found between $^1B_2$ and $^3B_2$ states. However, by using the complete active space self consistent field (CASSCF) and multireference configuration interaction (MRCI) methods, Spielfiedel *et al.*[12] found that there are surface crossing regions between $^1B_2$ and $^3B_2$ states at CO bond length $R_{CO} = 1.243$ Å and OCO bond angle in $90° < \alpha_{OCO} < 100°$. Spielfiedel *et al.*[12] also pointed out that the predissociation of $^1B_2$ state can occur through a triplet state $^3A_2$ intersection with the singlet state $^1B_2$. Therefore, it is still not very clear whether or not the $^1B_2$ state has intersection with $^3A_2$ state or/and $^3B_2$ state. The purpose of the present work is to study this problem and we try to carry out extensive high-level *ab initio* calculations for potential energy surfaces of the ground and excited states in order to understand the dissociation mechanism of carbon dioxide molecule. We have calculated PESs of the low-lying states $^1A_1$, $^1B_2$, $^1A_2$, $^3B_2$, and $^3A_2$ using the un-contracted MRCI method, and then we have fitted the calculated PESs into the analytical form to explore topology of intersections among these five low-lying electronic states.

The paper is organized as follows: in Sec. II we present a brief description of the high-level *ab initio* calculation methods and algorithm of analytical fitting to PES. Then we report detailed analysis and discussion of potential energy surfaces and related surface/conical intersections in Sec. III. Concluding remarks are given in Sec. IV.

a)Electronic mail: cyzhu@mail.nctu.edu.tw

 © 2013 AIP Publishing LLC

This article is copyrighted as indicated in the article. Reuse of AIP content is subject to the terms at: http://scitation.aip.org/termsconditions. Downloaded to IP: 140.113.38.11 On: Wed, 30 Apr 2014 06:05:21

II. COMPUTATIONAL METHODS

A. High-level *ab initio* calculations

The ground and several low-lying excited electronic state PESs of CO_2 are calculated at the un-contracted multi-reference configuration interaction with single and double excitation (MRCISD) level using the Xi'an-CI code.[13] The un-contracted MRCI(SD) method is based on the graphical unitary group approach (GUGA) and the hole-particle correspondence. The details of the method have been given in the original publications.[13–16] We utilized the state averaged CASSCF (SA-CASSCF) method with cc-pVTZ(6d, 10f) basis sets to generate the reference space by the GAMESS program package.[17] The multiconfiguration self-consistent field wave function consists of a complete configuration expansion for 12 electrons distributed in the 10 active valence orbitals. The active space CAS(12, 10) is chosen to have over 3000 configuration state functions (CSFs) under C_{2v} group symmetry and 7000 CSFs under C_s group symmetry. If all CAS configurations are chosen as the reference states in the MRCI(SD) calculation with the cc-pVTZ basis set, the number of CSFs can exceed 3.4×10^7 and 6.1×10^8 under C_{2v} and C_s group symmetry, respectively. It is extremely time-consuming for constructing potential energy surfaces under such high level calculation. In order to reduce computational cost, we only keep those CSFs with absolute coefficients larger than a preselected threshold in the reference space.

For instance, the number of CSFs in CI space is 34 964 540 without threshold selection, and it is reduced to 7 202 161 with the threshold set up to be 0.01 for ground state $^1A_1$ with CO bond length $R_{co} = 1.164$ Å and OCO angle $\alpha_{oco} = 180^\circ$. We found that the electronic energy of the ground state is −5119.4911 eV (−5120.0092 eV with Davidson correction) without the threshold selection, while it is −5119.4710 eV (−5120.0258 eV with Davidson correction) with 0.01 threshold selection. There is the correlation energy loss of 0.0201 eV with 0.01 threshold selection, but computation cost is reduced by 80%. For electronic triplet $^3B_2$ state, the number of CSFs in CI space is reduced to 7 804 228 from 64 665 634 by 0.01 threshold selection and the correlation energy loss is 0.0633 eV. We think that such small correlation energy loss is quite acceptable for potential energy surface calculations. On the other hand, we found that the electronic energy of the ground $^1A_1$ state is −5119.3967 eV calculated by internally contracted MRCI method implemented by Molpro software,[18,19] and this is 0.0955 eV higher than −5119.4911 eV obtained by the present un-contracted MRCI method. In general, the electronic energy calculated from internally contracted MRCI (ic-MRCI) is higher than that calculated from un-contracted MRCI method. This difference can become bigger while the basis set is smaller. In the following, all the calculations in the present work are based on un-contracted MRCI with the threshold selection 0.01.

One of the authors (Z.W.) has recently developed an improved version of the configuration-based multi-reference second-order perturbation approach (CB-MRPT2) according to the formulation of Lindgren on perturbation theory of a degenerate model space.[20] The diagonalize-then-perturb-then-diagonalize (DPD) model has been implemented and thus the DPD-MRPT2 method is considered to be an approximate MRCISD. It is most capable to rectify the shortcomings of the CASPT2 method.[21] Therefore, we also carried out the DPD-MRPT2 calculations in the present study.

B. Analytical fitting of potential energy surface

In order to explore topology of surface/conical intersections among the five low-lying electronic states, we fit the calculated PESs into the analytical functions. We apply the reproducing kernel Hilbert space (RKHS) method[22] to construct the analytical PESs. Two-dimensional (2D) analytical potential energy surface is constructed as a function V(R, θ) in which R is the CO bond length and θ is the OCO bond angle. Furthermore, we introduce the new variables $x = \alpha R$ (α is the scaling factor, and 0.5 is used in our calculations) and $y = (1 + \cos\theta)/2$, so that $0 \le x < \infty$ and $0 \le y \le 1$. We adopt the reciprocal power (RP) and Taylor spline (TS) reproducing kernel as follows:[23]

$$Q_{n_1,m_1;n_2}(x, y, x', y') = q^{RP}_{n_1,m_1}(x, x')q^{TS}_{n_2}(y, y'), \tag{1}$$

where $q^{RP}_{n_1,m_1}(x, x')$ is defined as

$$q^{RP}_{n,m}(x, x') = n^2 x_>^{-(m+1)} B(m+1, n)_2 \times F_1\left(-n+1, m+1; n+m+1, \frac{x_<}{x_>}\right) \tag{2}$$

in which $x_>$ and $x_<$ represent the larger and the smaller, respectively, for x and x'. B(a, b) is the beta function and ${}_2F_1(a, b; c; z)$ is the Gauss' hypergeometric function. The TS reproducing kernel is given by

$$q^{TS}_n(x, x') = \sum_{i=0}^{n-1} x^i x'^i + \xi^T_n(x, x') \tag{3}$$

and

$$\xi^T_n(x, x') = n x^n_< x_>^{n-1} F_1\left(1, -n+1; n+1; \frac{x_<}{x_>}\right). \tag{4}$$

We use $Q_{3,5;7}(x, y, x', y')$ with $n_1 = 3$, $m_1 = 5$, and $n_2 = 7$ in Eq. (1) to construct the 2D PESs of CO_2. This means that calculations are performed under the C_{2v} group symmetry. Each of the PESs is obtained from the completely filled 13 × 60 2D grids in which there are 780 *ab initio* data points for CO bond length in the region of [0.6, 2.37] Å with step interval 0.03 Å and the bond angle in the region of [60°, 180°] with step interval 10°. The overall root-mean-square (rms) error for the analytical PES is estimated as 0.0438 eV for $^1A_1$, 0.0846 eV for $^1A_2$, 0.0494 eV for $^1B_2$, 0.0403 eV for $^3B_2$, and 0.0503 eV for $^3A_2$.

III. RESULTS AND DISCUSSION

A. Vertical excitation energies

The ground state of CO_2 is in the linear geometry $^1\Sigma_g^+$ state with electronic configurations as

This article is copyrighted as indicated in the article. Reuse of AIP content is subject to the terms at: http://scitation.aip.org/termsconditions. Downloaded to IP: 140.113.38.11 On: Wed, 30 Apr 2014 06:05:21

TABLE I. Orbital space and main configurations of CO_2 for the ground state and the low-lying excited states in $D_{\infty h}$ and C_{2v} symmetry, respectively. Core orbitals ($1\sigma_g^2 1\sigma_u^2 2\sigma_g^2 2\sigma_u^2 3\sigma_g^2$) that are all doubly occupied are not shown here.

Orbital	6	7	8	9	10	11	12	13	14	15
C_{2v}	$4a_1$	$3b_2$	$1b_1$	$5a_1$	$1a_2$	$4b_2$	$6a_1$	$2b_1$	$7a_1$	$5b_2$
$D_{\infty h}$	$4\sigma_g$	$3\sigma_u$	$1\pi_u$	$1\pi_u$	$1\pi_g$	$1\pi_g$	$2\pi_u$	$2\pi_u$	$5\sigma_g$	$4\sigma_u$
$^1\Sigma_g^+(^1A_1)$	2	2	2	2	2	2	0	0	0	0
$^1\Sigma_u^-(1\text{-}^1A_2)$	2	2	2	2	1	2	1	0	0	0
$^1\Delta_u(2\text{-}^1A_2)$	2	2	2	2	2	1	0	1	0	0
$^1\Delta_u(1\text{-}^1B_2)$	2	2	2	2	1	2	0	1	0	0
	2	2	2	2	2	1	1	0	0	0
$^1\Pi_g(3\text{-}^1A_2)$	2	2	2	2	1	2	0	0	1	0
$^1\Pi_g(2\text{-}^1B_2)$	2	2	2	2	2	1	0	0	1	0
$^3\Sigma_u^+(1\text{-}^3B_2)$	2	2	2	2	2	1	1	0	0	0
$^3\Delta_u(2\text{-}^3B_2)$	2	2	2	2	1	2	0	1	0	0
$^3\Delta_u(1\text{-}^3A_2)$	2	2	2	2	1	2	1	0	0	0
$^3\Sigma_u^-(2\text{-}^3A_2)$	2	2	2	2	2	1	0	1	0	0
$^3\Pi_g(3\text{-}^3B_2)$	2	2	2	2	2	1	0	0	1	0
$^3\Pi_g(3\text{-}^3A_2)$	2	2	2	2	1	2	0	0	1	0

shown in Table I. The electronic configurations of the lowest excited states of CO_2 at linear geometry are $(1\sigma_g^2 1\sigma_u^2 2\sigma_g^2 2\sigma_u^2 3\sigma_g^2 3\sigma_u^2 4\sigma_g^2 1\pi_u^2 1\pi_u^2 1\pi_g^2 1\pi_g^1 2\pi_u^1)$ for Σ_u^-, Σ_u^+, Δ_u states and $(\cdots 1\pi_u^2 1\pi_u^2 1\pi_g^2 1\pi_g^1 5\sigma_g^1)$ for the Π_g states. The $5\sigma_g$ and $2\pi_u$ ($D_{\infty h}$ symmetry) are molecular orbitals corresponding to $6a_1$, $2b_1$, and $7a_1$, respectively, in C_{2v} group symmetry. The $5\sigma_g$ orbital has mixed valence-Rydberg character so that large augmented polarized basis set should be used. As pointed out by Spielfiedel,[12] in any electronic configuration in which either of these two a_1 orbital ($6a_1$, $7a_1$) are occupied, the energetically lower a_1 orbital always has more $2\pi_u$ character. The same conclusion is true for the triplet states. However, the behavior of these two a_1 states is opposite in singlet states $^1A_2$ and $^1B_2$. The orbital in $6a_1$ and $7a_1$ with higher energy has more $2\pi_u$ character. Thus, $5\sigma_g$ ($6a_1$) molecular orbital has lower energy than $2\pi_u$ ($2b_1$, $7a_1$) orbital at the $D_{\infty h}$ group symmetry.

The ground state of CO_2 in C_{2v} group symmetry is the $^1A_1$ state with electronic configurations (see Table I) $(1a_1^2 1b_2^2 2a_1^2 2b_2^2 3a_1^2 3b_2^2 4a_1^2 5a_1^2 1b_1^2 1a_2^2 4b_2^2)$. The B_2 states are correlated with $(4b_2^1 1a_2^2 6a_1^1)$, $(4b_2^2 1a_2^1 2b_1^1)$, and $(4b_2^1 1a_2^2 7a_1^1)$ configurations. It is found that the mixing of the $^1B_2$ configurations designated as $4b_2^1 1a_2^2 6a_1^1$ (1^1B_2) and $4b_2^2 1a_2^1 2b_1^1$ (2^1B_2) is required to ensure that the final $^1B_2$ states approach correctly into $^1\Pi_g$ and $^1\Delta_u$ states at linear geometry. In the calculation of triplet $^3B_2$ states, we optimize $^3B_2$ states by a state-average of all the three states. The A_2 states are correlated with $(4b_2^2 1a_2^1 6a_1^1)$, $(4b_2^2 1a_2^1 7a_1^1)$, and $(4b_2^1 1a_2^2 2b_1^1)$ configurations. Similarly, we optimize $^3A_2$ states in a state-averaged procedure with the same weight. The $^3A_2$ states and $^3B_2$ states succeed to converge to the $^3\Delta_u$ and $^3\Pi_g$ states, respectively, as shown in Fig. 1. For the $^1A_2$ states, the computed $^1A_2$ state approaches to $^1\Delta_u$ and $^1\Sigma_u^-$ states correctly if the configurations are designated as the mixing of 1^1A_2 and 2^1A_2 states. But if three-state average procedure is used during the optimization, the results

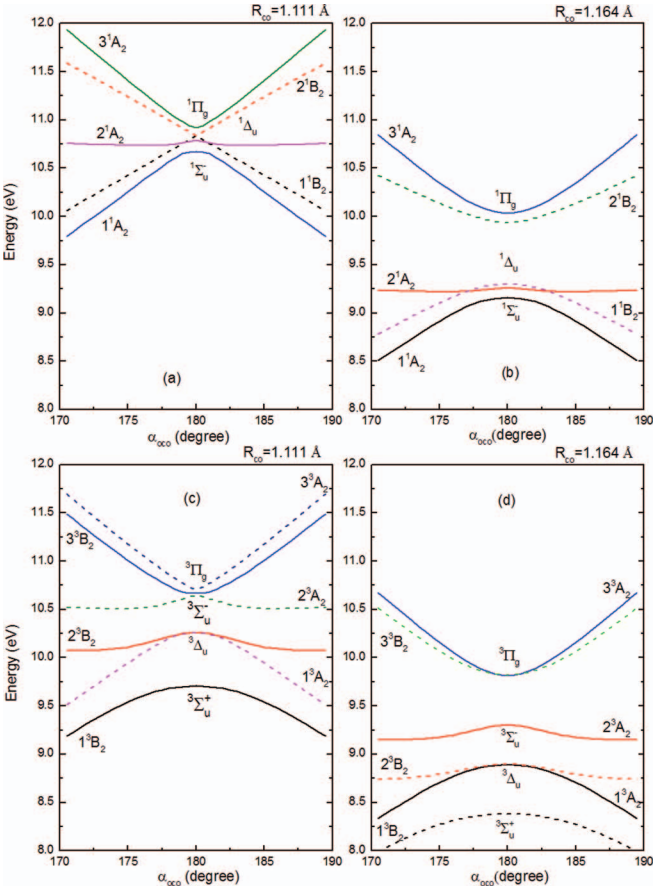

FIG. 1. The one-dimensional potential energy curves for the low-lying excited states of CO_2 along the bond angle in the region of $190^\circ > \alpha_{oco} > 170^\circ$ at fixed bond length $R_{co} = 1.111$ Å and 1.164 Å, respectively. (a) At $R_{co} = 1.111$ Å for singlet states, the solid lines correspond to $^1A_2$ and dashed lines correspond to $^1B_2$. (b) The same as (a) except at 1.164 Å. (c) At $R_{co} = 1.111$ Å for triplet states, the solid lines correspond to $^3B_2$ and dashed lines correspond to $^3A_2$. (d) The same as (c) except at $R_{co} = 1.164$ Å.

converge to

$$\tilde{X}\begin{cases} 4a_1^2 3b_2^2 5a_1^2 1b_1^2 4b_2 1a_2^2 2b_1(0.6358) \\ 4a_1^2 3b_2^2 5a_1^2 1b_1^2 4b_2^2 1a_2 7a_1(0.6802) \end{cases},$$

$$\tilde{A}\begin{cases} 4a_1^2 3b_2^2 5a_1^2 1b_1^2 4b_2 1a_2^2 2b_1(-0.6766) \\ 4a_1^2 3b_2^2 5a_1^2 1b_1^2 4b_2^2 1a_2 7a_1(0.6362) \end{cases},$$

and

$$\tilde{B}\ \{4a_1^2 3b_2^2 5a_1^2 1b_1^2 4b_2^2 1a_2 6a_1(0.9146)\ .$$

The $\tilde{X}$, $\tilde{A}$, and $\tilde{B}$ states correspond to the $^1\Sigma_u^-$, $^1\Delta_u$, and $^1\Pi_g$ states, respectively. While the two $^1B_2$ states succeed to converge to the $\tilde{X}$ ($^1\Delta_u$ at 180°) and $\tilde{A}$ ($^1\Pi_g$ at 180°) as follows:

$$\tilde{X}\begin{cases} 4a_1^2 3b_2^2 5a_1^2 1b_1^2 1a_2^2 4b_2 7a_1(0.6598) \\ 4a_1^2 3b_2^2 5a_1^2 1b_1^2 1a_2 4b_2^2 2b_1(0.6526) \end{cases}$$

and

$$\tilde{A}\ \{4a_1^2 3b_2^2 5a_1^2 1b_1^2 1a_2^2 4b_2 6a_1(-0.9212)\ .$$

This causes that energy of the $^1\Delta_u$ state is about 0.04 eV higher estimated from $^1A_2$ than from $^1B_2$ state. The energy of $^1\Pi_g$ state is about 0.10 eV lower estimated from $^1A_2$ than

This article is copyrighted as indicated in the article. Reuse of AIP content is subject to the terms at: http://scitation.aip.org/termsconditions. Downloaded to IP: 140.113.38.11 On: Wed, 30 Apr 2014 06:05:21

TABLE II. Vertical excitation energies of CO_2 for $R_{co} = 1.164$ Å (2.20 Bohr) and $\alpha_{oco} = 180°$, and all energies are relative to the energy of the electronic ground state $E(^1A_1) = -5119.4704$ eV. (-5120.0255 eV with Davidson correction) at linear geometry.

States						
$D_{\infty h}$	C_{2v}	MRCI (0.00)	MRCI + Q[a]	MRCI(0.01)[b]	MRCI + Q	DPD-MRPT2
$^3\Sigma_u^+$	$^3B_2$	8.27	8.19	8.38(8.35[c])	8.15	8.23
$^3\Delta_u$	$^3A_2$	8.77	8.72	8.81(8.83)	8.56	8.77
	$^3B_2$	8.79	8.73	8.84(8.83)	8.80	8.77
$^3\Sigma_u^-$	$^3A_2$	9.16	9.14	9.22(9.21)	9.18	9.20
$^3\Pi_g$	$^3A_2$	9.71	9.55	9.77(8.61)	9.54	10.05
	$^3B_2$	9.71	9.52	9.82(8.61)	9.58	10.09
$^1\Sigma_u^-$	$^1A_2$	9.14	9.11	9.17(9.19)	8.90	9.19
$^1\Delta_u$	$^1A_2$	9.25	9.17	9.28(9.28)	9.26	9.30
	$^1B_2$	9.48	9.38	9.48(9.28)	9.34	9.45
$^1\Pi_g$	$^1A_2$	10.00	10.25	10.10(9.00)	9.89	10.42
	$^1B_2$	9.92	9.84	10.09(9.00)	9.88	10.17

[a]Un-contracted MRCI method with Davidson correction (+Q).
[b]Un-contracted MRCI method with the reference configuration threshold selection set up to be 0.01.
[c]The theoretical results from Spielfiedel's work[12] with internally contracted MRCI method.

from $^1B_2$ state. We also notice that the equilibrium geometry of $^1\Pi_g$ state ($3^1A'$ and $3^1A''$) is linear with nonsymmetrical CO bond lengths under C_s symmetry.

The vertical excitation energies are summarized in Table II with the comparison to theoretical work of Spielfiedel *et al.*[12] The present results are inconsistent with the recent work by Grebenshchikov,[24] in which the vertical excitation energies are in the order of $E(^1\Sigma_u^-) < E(^1\Delta_u) < E(^1\Pi_g)$ based on larger basis set and internally contracted MRCI method. This is different from Knowles[25] and Spielfiedel *et al.*'s[12] work which gives the order of $E(^1\Pi_g) < E(^1\Sigma_u^-) < E(^1\Delta_u)$. For the triplet states, vertical excitation energies are in the order of $E(^3\Sigma_u^+) < E(^3\Delta_u) < E(^3\Pi_g) < E(^3\Sigma_u^-)$ from the present calculation and it is different from Spielfiedel *et al.*'s[12] work in the order of $E(^3\Sigma_u^+) < E(^3\Delta_u) < E(^3\Sigma_u^-) < E(^3\Pi_g)$.

For the adiabatic excitation energies, both the present and Spielfiedel *et al.*'s[12] methods turn out to be 5.53 eV and 5.80 eV (5.62 eV and 5.88 eV with configuration selection) for $^1A_2$ and $^1B_2$, respectively. This is in agreement with Clyne and Thrush's suggestion[26] that the first excited singlet states of CO_2 are bent $^1A_2$ and $^1B_2$ states which are fairly similar in adiabatic excitation energy. The equilibrium bond length of $^1A_1$ state in the present calculation is 1.162 Å that is slightly longer than the experimental value 1.160 Å.[27] The equilibrium geometries of the lowest $^{1,3}A_2$ and $^{1,3}B_2$ states calculated from available MRCISD methods are summarized in Table III. It is only $^1B_2$ state that can be directly compared with the experimental values. In Dixon's classical work,[28] the rotational structures of $^1B_2$ state have been detected, and the equilibrium geometry of $^1B_2$ state is estimated as bond length $R_{co} = 1.246 \pm 0.008$ Å and bond angle $\alpha_{OCO} = 122° \pm 2°$. The present calculation predicted $R_{co} = 1.255$ Å and $\alpha_{OCO} = 118.0°$ for $^1B_2$ state and it is in reasonable agreement with the experimental value. As shown in Table III, the excitation energy from un-contracted MRCISD method is closest to the experimental value. The differences of vertical excitation energies between un-contracted and internally contracted MRCISD methods are in the range of 0.01 to 0.22 eV. The energy differences induced by the configuration selection are in the range of 0.05 to 0.23 eV. The present un-contracted MRCISD method without configuration selection gives the lower excitation energy as compared with the internally contracted MRCISD methods.

Furthermore, we carried out the DPD-MRPT2 calculations to conform that both un-contracted MRCI and

TABLE III. Optimized geometries of the low-lying bent excited states of CO_2 with available MRCISD methods.

States	Methods	Geometry		Dimension of CI spaces	E_{mrci} (eV)
		R_{co} (Å)	α_{oco} (°)		
$^1B_2$	MRCISD[a]	1.255	118.0	34909004	5.80
	MRCISD(0.01)[b]	1.265	118.5	6201153	5.88
	ic-MRCISD[c]	1.254	118.0	666920	5.83
	ic-MRCISD(0.01)[d]	1.258	117.1	374383	6.06
	Expt.[e]	1.246	122.0		5.70
$^1A_2$	MRCISD	1.252	127.0	34657216	5.53
	MRCISD(0.01)	1.255	127.5	11583986	5.62
	ic-MRCISD	1.254	127.4	737290	5.54
	ic-MRCISD(0.01)	1.253	127.4	562053	5.53
$^3B_2$	MRCISD	1.245	118.5	64665634	4.66
	MRCISD(0.01)	1.251	114.0	13362429	4.83
	ic-MRCISD	1.247	118.2	1110878	4.88
	ic-MRCISD(0.01)	1.242	119.0	658302	4.72
$^3A_2$	MRCISD	1.254	127.3	64259728	5.32
	MRCISD(0.01)	1.250	129.0	22097203	5.37
	ic-MRCISD	1.254	127.7	1111126	5.35
	ic-MRCISD(0.01)	1.253	127.7	825967	5.33

[a]Un-contracted MRCISD method from the Xi'an CI program.
[b]Un-contracted MRCISD method with configuration selection (threshold 0.01) from the Xi'an CI program.
[c]Internally contracted MRCISD method from the MOLPRO program suite.[18]
[d]Internally contracted MRCISD method with configuration selection (threshold 0.01) from the MOLPRO program suite.[18]
[e]Experimental values from Dixon's work.[28]

This article is copyrighted as indicated in the article. Reuse of AIP content is subject to the terms at: http://scitation.aip.org/termsconditions. Downloaded to IP: 140.113.38.11 On: Wed, 30 Apr 2014 06:05:21

DPD-MRPT2 methods give the same order for excitation energies as shown in Table II and Table S1 in supplementary material.[34] We believe that the present un-contracted MRCI method predicted correct order of vertical excitation energies for the lower excited states.

B. 1D potential energy curves for bent valence excited states of CO_2

We first carried out calculations for the one-dimensional potential curves in the region of the bond angle $190^\circ > \alpha_{oco} > 170^\circ$ at fixed bond length $R_{co} = 1.111$ and $R_{co} = 1.164$ Å, respectively, for the low-lying excited states. 1D potential curves are plotted in Fig. 1. We found that the lowest $^1B_2$ state ($^1\Pi_g$ at 180°) forms a conical intersection with the second $^1B_2$ state ($^1\Delta_u$ at 180°) at $R_{co} = 1.111$ Å.

For three singlet $^1A_2$ states, the dominating configurations are $(4b_2^2 1a_2^1 6a_1^1)$, $(4b_2^1 1a_2^2 2b_1^1)$, and $(4b_2^2 1a_2^1 7a_1^1)$ in energy sequence, the 3-$^1A_2$ (1-$^1A_2$) has local minimum (maximum) at OCO angle around 180° where these two states form an avoided crossing, while the 2-$^1A_2$ state is almost unchanged in bond angle $190^\circ > \alpha_{oco} > 170^\circ$ as shown in Figs. 1(a) and 1(b).

For the triplet states of CO_2, the conical intersection is formed between the 2-$^3A_2$ and 3-$^3A_2$ at $R_{co} = 1.111$ Å and $\alpha_{oco} = 180^\circ$ as shown in Fig. 1(c), and three triplet $^3B_2$ states have similar behavior to their counterpart of three singlet $^1A_2$ states. Especially, the dominating configurations are also the same. Both 3-$^3A_2$ (1-$^3A_2$) and 3-$^3B_2$ (2-$^3B_2$) states correctly approach to $^3\Pi_g$ ($^3\Delta_u$) state at linear geometry. An avoided crossing is formed between the 3-$^3B_2$ and 2-$^3B_2$ states at R_{co} slightly short than 1.111 Å and $\alpha_{oco} = 180^\circ$ as shown in Fig. 1(c).

We again carried out DPD-MRPT2 calculations for conical intersections and avoided crossings for both low-lying singlet and triplet states, and detailed information is shown in Figs. S1, S2, S3, S4, and S5 in supplementary material.[34] DPD-MRPT2 calculations basically conform what we have obtained from un-contracted MRCI calculations discussed above. Besides, the 2-$^1A_2$, 2-$^3A_2$, and 2-$^3B_2$ states, which are predominantly described by the electronic configurations involving the b_1 component of the $2\pi_u$ molecular orbital, have only very small barriers at linear geometry. This complicates photodissociation of CO_2 by the fact that the valence singlet and triplet states $^{1,3}\Sigma_u^-$ and $^{1,3}\Delta_u$ form conical intersections with the diffuse $^{1,3}\Pi_g$ states in the Franck-Condon region of the absorption spectrum.

C. 2D potential energy surfaces for bent valence excited states of CO_2

We next carried out calculations for the two-dimensional potential contours in terms of bond lengths R_{co} and the OCO angle α_{oco} under C_{2v} group symmetry. Then we utilized analytical fitting method introduced in Sec. II B to obtain analytical potential energy surfaces for the ground state $^1A_1$, and the low-lying excited states $^1A_2$, $^3A_2$, $^1B_2$, and $^3B_2$ as plotted in Fig. 2.

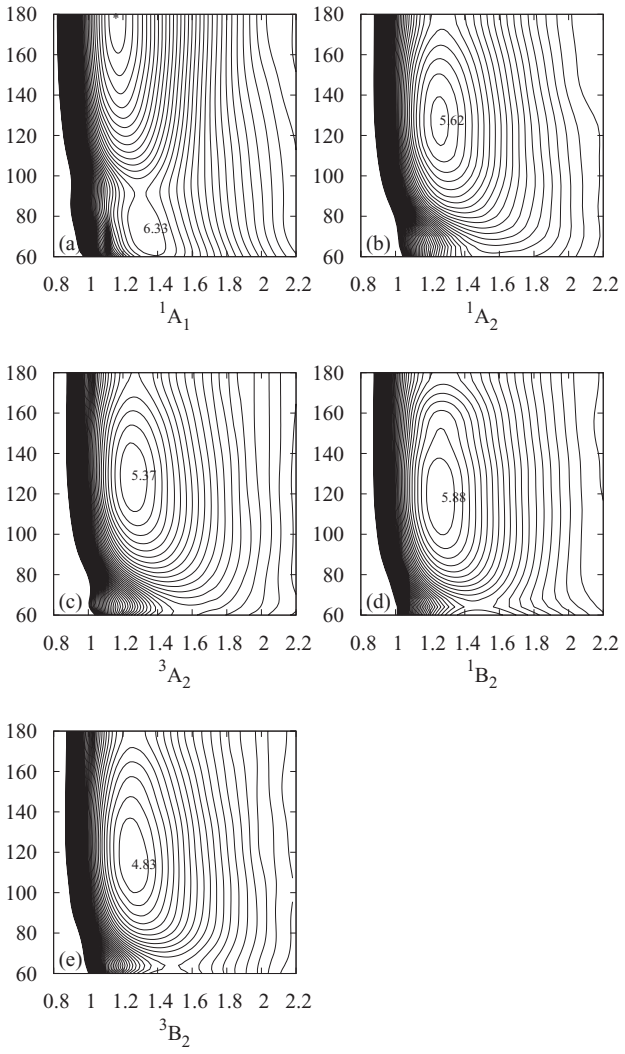

FIG. 2. Contour plot of the fitted potential energy surfaces for the low-lying electronic states (a) $^1A_1$, (b) $^1A_2$, (c) $^3A_2$, (d) $^1B_2$, and (e) $^3B_2$. The two axes are the bond lengths R_{co} in Å, and the OCO angle α_{oco} in degree. The minimal values of the potential energy surfaces have been plotted in eV with respect to the ground-state $^1A_1$ minimum. The contour increment is 0.05 eV.

We found that the ground state potential energy surface has a double-well structure with the global minimum at bond length $R_{co} = 1.162$ Å (linear geometry) and local bent minimum at $R_{co} = 1.32$ Å and $\alpha = 73.4^\circ$. There is an energy gap of 6.33 eV between the two minima. The C_{2v} constrained saddle point that was found at $R_{co} = 1.30$ Å and $\alpha = 91^\circ$ connects these two minima with potential barrier of 0.433 eV above the bent minimum. The transition state of the ground state is very close to the local bend minimum. The present calculation is basically in agreement with the result obtained by Xantheas and Ruedenberg,[29] which estimate the saddle point at $R_{co} = 1.32$ Å and $\alpha = 94.2^\circ$ with a potential barrier of 0.607 eV above the local bend minimum. All other four excited states $^1A_2$, $^3A_2$, $^1B_2$, and $^3B_2$ are quite similar to the ground state $^1A_1$, and they all have double-well structures. The local minima of $^1A_2$ and $^1B_2$ states are located at smaller bond angle ($\alpha_{OCO} < 60^\circ$) which are out of the plotted region in Fig. 2.

This article is copyrighted as indicated in the article. Reuse of AIP content is subject to the terms at: http://scitation.aip.org/termsconditions. Downloaded to IP: 140.113.38.11 On: Wed, 30 Apr 2014 06:05:21

D. The topology of surface/conical intersections among $^1A_1$, $^1A_2$, $^3A_2$, $^1B_2$, and $^3B_2$ states

We finally exhibited the topology of intersections among five electronic states $^1A_1$, $^1A_2$, $^3A_2$, $^1B_2$, and $^3B_2$, and we analyzed the reaction pathways via those surface intersections. It should be noted that the $^3B_2$ state is the lowest triplet state of CO_2 and it is correlated to the lowest $^3A'$ and $^3\Sigma_u^+$ states in C_s and $D_{\infty h}$ group symmetry, respectively.

The surface crossing between $^1A_1$ and $^3B_2$ states has the great influence on the dynamical behavior of O–CO reaction. We found that this singlet-triplet surface crossing of $^1A_1$ and $^3B_2$ states occurs at CO bond length $R_{co} > 1.6$ Å when the OCO angle is larger than 120°, as shown in Fig. 3(a). There is an interesting area for surface crossing from bond angle 85° to 105°, within which the $^3B_2$ surface is always below the $^1A_1$ surface for any bond length, and this special area has energy about 5.4 eV above the ground state. It should be noted that $^3B_2$ state at the equilibrium geometry has energy just 4.85 eV above the ground state. This special area is very close to the photodissociation threshold that has energy 5.45 eV above the ground state.[30] It is well known that the singlet and triplet potential energy surface crossing happens as the elongation of CO bond length ($R_{co} > 1.6$ Å).[4] The present calculation shows that the bending vibration mode at high quantum number can also lead to the singlet and triplet surfaces crossing, and it results in another pathway for the relaxation of CO + O(^{3}P) system.

The crossing between $^1B_2$ and $^3B_2$ states also has the great importance in understanding the photodissociation process of CO_2. From Simkin *et al.*'s MRCI calculation,[11] no crossing point is found between $^1B_2$ and $^3B_2$ states. On the other hand, from Spielfiedel *et al.*'s MRCI calculation,[12] the crossing area is found at the bond length 1.243 Å and bond angle from 90° to 100°. The present calculation does show crossing region around bond length 1.0 Å and bond angle 180° as plotted in Fig. 3(b), and otherwise the $^1B_2$ state has potential energy higher than the $^3B_2$ state. This area is very close to the conical intersection point of the first and second $^1B_2$ state reported in Sec. III B, and thus it can play an important role in the photodissociation process of CO_2. However, the area of surface intersection between $^1B_2$ and $^3B_2$ has energy about 13 eV above the $^1A_1$ ground state. From the present calculations, we notice that the energy difference between the $^1B_2$ and $^3B_2$ states is small (smaller than 1.0 eV) when the OCO angle is smaller than 140°. Vibrational excitation is very important when the interaction between these two states is taken into account. This makes the interaction of $^1B_2$ and $^3B_2$ surfaces complicated. At about $A_{oco} = 120°$ which is close to the minimum of $^3B_2$ states, the energy level is in

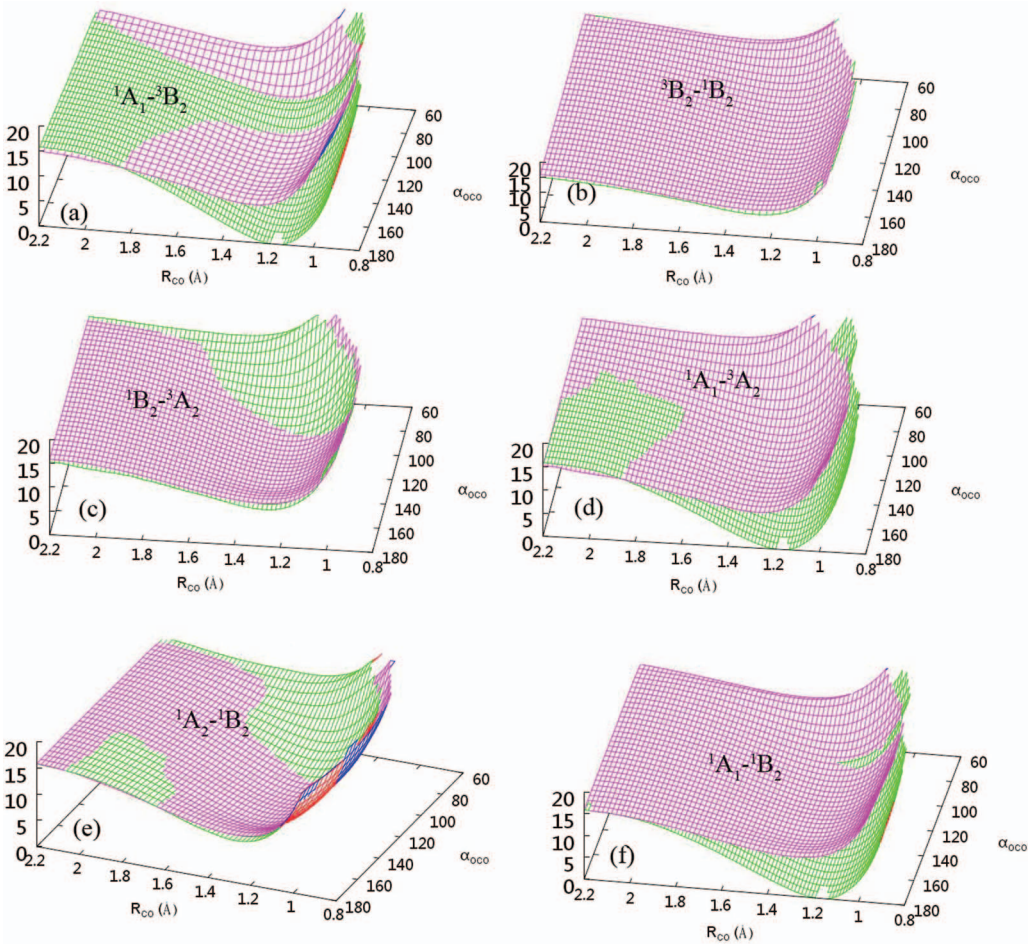

FIG. 3. The topology of conical intersections between (a) $^1A_1$ and $^3B_2$ states, (b) $^3B_2$ and $^1B_2$ states, (c) $^1B_2$ and $^3A_2$ states, (d) $^1A_1$ and $^3A_2$ states, (e) $^1A_2$ and $^1B_2$ states, and (f) $^1A_1$ and $^1B_2$ states. The z axis is the energy in eV. The x axis is the bond length in Å and the y axis is the OCO bond angle in degree.

This article is copyrighted as indicated in the article. Reuse of AIP content is subject to the terms at: http://scitation.aip.org/termsconditions. Downloaded to IP: 140.113.38.11 On: Wed, 30 Apr 2014 06:05:21

the region of 5.0–6.0 eV, which is consistent with the surface intersection area (5.72 eV) suggested by Lin's work[31] and Kinnersley's work.[32] From this point of view, the present results agree with the experiments and thus we present an alternative interaction mechanism. The detailed analysis is shown in Fig. S6 of supplementary material.[34]

The surface crossing between $^1B_2$ and $^3A_2$ states is found to occur in two regions as shown in Fig. 3(c); one is near the linear structure and bond length $R_{co} < 1.05$ Å and another is in the region at bond angle $\alpha_{OCO} < 140°$. Therefore, we think that the predissociation of $^1B_2$ state may occur through surface crossing between triplet state $^3A_2$ and the singlet state $^1B_2$.

We found that the $^3A_2$ state has energy always higher than the $^3B_2$ states, and there is no crossing between these two states. The $^3A_2$ and $^3B_2$ states became degenerate at CO bond length $R_{co} > 2.3$ Å. However, the $^3A_2$ surface has crossing with the $^1A_1$ surface in the region at the bond angle $\alpha_{oco} > 118°$ and bond length $R_{co} > 1.85$ Å as shown in Fig. 3(d).

The present calculation shows complicated topology pattern of surface crossing between $^1A_2$ and $^1B_2$ states, and these two potential surfaces are quite close in energy as shown in Fig. 3(e). We do not find crossing point between $^1A_1$ and $^1A_2$ states. On the other hand, we did find conical intersection between the $^1A_1$ and $^1B_2$ states, which takes place in the region of $R_{co} < 1.2$ Å and $92° < \alpha_{oco} < 100°$ as shown in Fig. 3(f). This crossing area is overlapped with the crossing area between $^3B_2$ and $^1A_1$ states.

In order to demonstrate important reaction pathways, we plot the crossing seams in Fig. 4 between the $^1A_1$ and $^3B_2$ states, the $^1B_2$ and $^3A_2$ states, and the $^1B_2$ and $^1A_2$ states. We found there are double crossing seams between the $^1A_1$ and $^3B_2$ states as shown in Fig. 4(a), the lower seam has energy 4.89 eV above the ground state at local minimum of the geometry $R_{co} = 1.28$ Å and $\alpha_{oco} = 108°$, while the upper seam has energy 6.63 eV above ground state at local minimum corresponding to the geometry $R_{co} = 1.33$ Å, $\alpha_{oco} = 85.6°$. There is only one crossing seam between $^1B_2$ and $^3A_2$ states as shown in Fig. 4(b), and it has energy 5.95 eV above the ground state at local minimum $R_{co} = 1.25$ Å and $\alpha_{oco} = 109°$. The crossing seam of $^1A_2$ and $^1B_2$ have three parts, one is bond length $R_{co} > 1.61$ Å and $\alpha_{oco} > 150°$ with the energy 11.0 eV above the global minimum. The second is $R_{co} < 1.0$ Å and $\alpha_{oco} > 150°$ with the energy 15.9 eV above the global minimum. The third is the continuous seam as bond angle smaller than 140° as shown in Fig. 4(c), and it has energy 5.92 eV above the ground state at local minimum of $R_{co} = 1.25$ Å and $\alpha_{oco} = 113°$. This means that the crossing points for these two pairs (one is $^1B_2$ and $^3A_2$, and another is $^1A_2$ and $^1B_2$) are quite close in both energy and geometry. We found there is energy jump at $R_{co} = 1.64690$ Å as shown in attached window of Fig. 4(c) and we have analyzed that this is due to projection from two dimensions (see Fig. 3(e)) to one dimension.

We conclude from the present study that the predissociation of $^1B_2$ state can occur through the surface intersection between the triplet $^3B_2$ state and the singlet $^1B_2$ state, and through the intersection between the triplet $^3A_2$ state and the singlet $^1B_2$ state. It has been known for a long time that all these states can predissociate in linear structures.[33] However, we found that there are even more predissociation pathways from bent geometry as shown in Figs. 3 and 4.

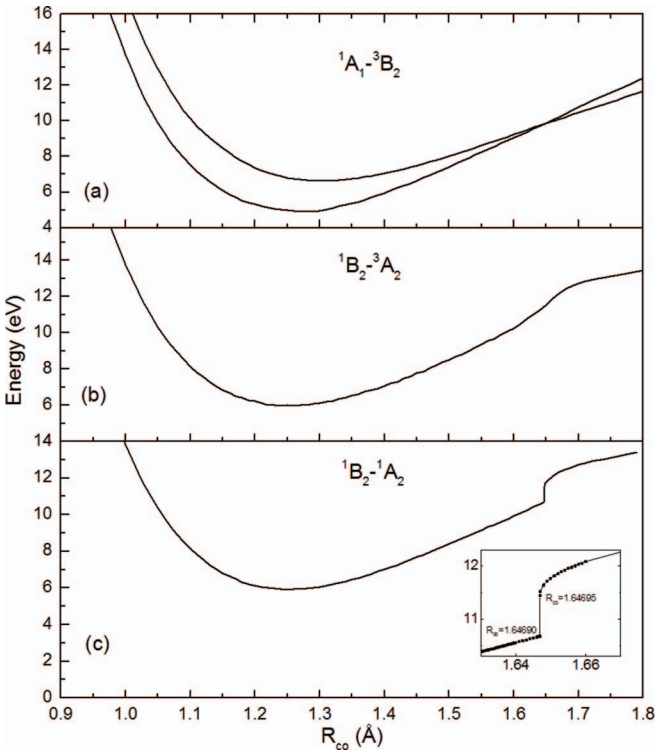

FIG. 4. Conical intersection seam lines between (a) the $^1A_1$ and $^3B_2$ states, (b) the $^1B_2$ and $^3A_2$ states, and (c) the $^1B_2$ and $^1A_2$ states, which are corresponding to Figs. 3(a), 3(c), and 3(e), respectively. The seam plotted in (c) represents the intersection of $^1B_2$ and $^1A_2$ states when the OCO bond angle less than 140°. All energies are relative to the global minimal of the ground state ($^1A_1$ state). The bond length is given in Angstrom, and the energy is in eV.

IV. CONCLUDING REMARKS

Un-contracted MRCISD method has been used to calculate the potential energy surfaces of the five low-lying electronic states $^1A_1$, $^1A_2$, $^3A_2$, $^1B_2$, and $^3B_2$ of CO_2. By applying the reproducing kernel Hilbert space method to fit potential energy surfaces of these five low-lying states in the analytical forms, we demonstrated topology of the conical/surface intersections near the equilibrium geometry of these five states. We first confirmed that the vertical excitation energies from the present high-level calculations agree with the recent high-level MRCI calculations, and we also noticed the deviations from the early internally contracted MRCI works. Then we extended the present un-contracted MRCI method to calculate conical/surface intersections in both linear geometry and bend geometry of CO_2. We found that conical intersection between singlet $^1\Delta_u$ and $^1\Pi_g$ states in the case of linear geometry corresponds to conical intersection between the first and second $^1B_2$ states in the case of bend geometry at bond length $R_{co} = 1.111$ Å. Actually, we found that the conical intersection between triplet $^3\Delta_u$ and $^3\Pi_g$ states occurs at the same region of the corresponding two singlet states. In the case of bend geometry, we found that the dissociation of $O(^3P)$ + CO can occur through the surface intersection between $^3B_2$

This article is copyrighted as indicated in the article. Reuse of AIP content is subject to the terms at: http://scitation.aip.org/termsconditions. Downloaded to IP: 140.113.38.11 On: Wed, 30 Apr 2014 06:05:21

and $^1B_2$ states, and the surface intersection between $^3A_2$ and $^1B_2$ states. The ground state $^1A_1$ has a large area of intersection with the lowest triplet $^3B_2$ state around bond angle at 95°, and this provides a potentially wide-region relaxation pathways. The $^1B_2$ state also has a small intersection region with the $^1A_1$ state around $R_{co} < 1.2$ Å and $\alpha_{oco} = 95°$. This makes the relaxation mechanism of $^1B_2$ state more complicated than the previous works. We have used the newly developed DPD-MRPT2 method to confirm the calculations from the un-contracted MRCI method and this makes the present high-level calculations in solid base for conical/surface intersections. In the near future, we need to do un-contracted MRCI calculations for potential energy surfaces in C_s symmetry and trajectory surface hopping must be performed for quantitatively studying dissociation reaction of CO_2.

ACKNOWLEDGMENTS

B. Zhou would like to thank Postdoctoral Fellowship supported by National Science Council of the Republic of China under Grant No. 100-2811-M-009-056. This work is supported by National Science Council of the Republic of China under Grant No. 100-2113-M-009-005-MY3. C. Zhu would like to thank the MOE-ATU project of the National Chiao Tung University for support.

[1]R. E. Center, J. Chem. Phys. **58**, 5230 (1973).
[2]M. E. Lewittes, C. C. Davis, and R. A. McFarlane, J. Chem. Phys. **69**, 1952 (1978).
[3]M. Abe, Y. Inagaki, L. L. Springsteen, Y. Matsumi, and M. Kawasaki, J. Phys. Chem. **98**, 12641 (1994).
[4]D. R. Harding, R. E. Weston, Jr., and G. W. Flynn, J. Chem. Phys. **88**, 3590 (1988).
[5]M. Braunstein and J. W. Duff, J. Chem. Phys. **112**, 2736 (2000).
[6]H. C. Chiang, N.-S. Wang, S. Tsuchiya, H.-T. Chen, Y.-P. Lee, and M. C. Lin, J. Phys. Chem. A **113**, 13260 (2009).
[7]C. Park, *Nonequilibrium Hypersonic Aerothermodynamics* (Wiley-Interscience, New York, 1990), pp. 57–60.
[8]T. G. Slanger, R. L. Sharpless, G. Black, and S. V. Filseth, J. Chem. Phys. **61**, 5022 (1974).
[9]S. Mahata and S. K. Bhattacharya, J. Chem. Phys. **130**, 234312 (2009).
[10]P. S. Julienne, D. Neuman, and M. Kraus, J. Atmos. Sci. **28**, 833 (1971).
[11]V. Y. Simkin, A. 1. Dementev, and Y. I. Pupyshev, Russ. J. Phys. Chem. **56**, 1739 (1982).
[12]A. Spielfiedel, N. Feautrier, C. Cossart-Magos, G. Chambaud, P. Rosmus, H. J. Werner, and P. Botschwina, J. Chem. Phys. **97**, 8382 (1992).
[13]Y. Wang, G. Zhai, B. Suo, Z. Gan, and Z. Wen, Chem. Phys. Lett. **375**, 134 (2003).
[14]Y. Wang, Z. Wen, Q. Du, and Z. Zhang, J. Comput. Chem. **13**, 187 (1992); B. Suo, G. Zhai, Y. Wang, Z. Wen, X. Hu, and L. Li, *ibid.* **26**, 88 (2005).
[15]A. Li, H. Han, B. Suo, Y. Wang, and Z. Wen, Sci. China Chem. **53**, 933 (2010); Y. Wang, Z. Gan, K. Su, and Z. Wen, Sci. China, Ser. B: Chem. **43**, 567 (2000).
[16]H. Han, B. Suo, D. Xie, Y. Lei, Y. Wang, and Z. Wen, Phys. Chem. Chem. Phys. **13**, 2723 (2011).
[17]GAMESS version (11 August 2011) M. W. Schmidt, K. K. Baldridge, J. A. Boatz, M. S. Gordon, J. H. Jensen, S. Koseki, N. Matsunaga, K. A. Nguyen, S. J. Su, T. L. Windus, M. Dupuis, and J. A. Montgomery, J. Comput. Chem. **14**, 1347 (1993).
[18]H.-J. Werner, P. J. Knowles, G. Knizia, F. R. Manby, M. Schütz *et al.*, MOLPRO, version 2010.1, a package of *ab initio* programs, 2010, see http://www.molpro.net.
[19]H.-J. Werner and P. J. Knowles, J. Chem. Phys. **89**, 5803 (1988).
[20]I. Lindgren and J. Morrison, *Atomic Many-Body Theory* (Springer-Verlag, Berlin, 1982).
[21]Y. Lei, Y. Wang, H. Han, Q. Song, B. Suo, and Z. Wen, J. Chem. Phys. **137**, 144102 (2012).
[22]T.-S. Ho and H. Rabitz, J. Chem. Phys. **104**, 2584 (1996).
[23]T. Hollebeek, T.-S. Ho, and H. Rabitz, Annu. Rev. Phys. Chem. **50**, 537 (1999).
[24]S. Yu. Grebenshchikov, J. Chem. Phys. **137**, 021101 (2012).
[25]P. J. Knowles, P. Rosmus, and H.-J. Werner, Chem. Phys. Lett. **146**, 230 (1988).
[26]M. A. A. Clyne and B. A. Thrush, Proc. R. Soc. London, Ser. A **269**, 404 (1962).
[27]R. B. Wattson and L. S. Rothman, J. Mol. Spectrosc. **119**, 83 (1986).
[28]R. N. Dixon, Proc. R. Soc. London, Ser. A **275**, 431 (1963).
[29]S. S. Xantheas and K. Ruedenberg, Int. J. Quantum Chem. **49**, 409 (1994).
[30]E. C. Y. Inn, K. Watanabe, and M. Zelikoff, J. Chem. Phys. **21**, 1648 (1953).
[31]R. G. Shortridge and M. C. Lin, J. Chem. Phys. **64**, 4076 (1976).
[32]S. R. Kinnersly, Mol. Phys. **38**, 1067 (1979).
[33]H. Okabe, *Photochemistry of Small Molecules* (Wiley, New York, 1978).
[34]See supplementary material at http://dx.doi.org/10.1063/1.4824483 for including details from the DPD-MRPT2 calculations. This includes optimized geometries, order of energy levels of singlet and triplet states, and conical intersections among those low-lying states in comparison with MRCI calculations.

This article is copyrighted as indicated in the article. Reuse of AIP content is subject to the terms at: http://scitation.aip.org/termsconditions. Downloaded to IP: 140.113.38.11 On: Wed, 30 Apr 2014 06:05:21